Supporting Information

Metal-organic framework-derived Co single atoms anchored on N-doped hierarchically porous carbon as a pH-universal ORR electrocatalyst for Zn-air batteries

Le Li[1,2], *Na Li*[1], *Jiawei Xia*[1], *Shilong Zhou*[1], *Xingyue Qian*[1], *Fengxiang Yin*[1], *Guangyu He*[1,*], *Haiqun Chen*[1,*]

[1] Key Laboratory of Advanced Catalytic Materials and Technology, Advanced Catalysis and Green Manufacturing Collaborative Innovation Center, Changzhou University, Changzhou 213164, China

[2] Jiangsu Urban and Rural Construction Vocational College, Changzhou, 213147, China

E-mail: hegy@cczu.edu.cn (G. He), chenhq@cczu.edu.cn (H. Chen)

1 Experimental section

1.1 Materials Characterization

The morphologies of the materials were characterized by scanning electron microscopy (SEM, Zeiss Sigma 300 Cold Field scanning electron microscope), transmission electron microscopy (TEM, JEOL JEM-2100F, performed at U_0 = 200 kV), and aberration corrector high-angle annular dark-field scanning transmission electron microscopy (AC-HAADF-STEM, FEI Theims Z, performed at 300 kV with a probe spherical aberration corrector). The crystalline structures of the materials were analyzed via X-ray diffraction (XRD) patterns recorded on a Rigaku Ultima IV X-ray diffractometer (Cu Kα, λ = 0.15418 nm) with a scanning range of 2θ from 10 to 80°. Raman spectra were recorded on a Thermo Fischer DXR Evolution spectrometer at a laser wavelength of 633 nm. Specific surface area and porous structure information were obtained according to N_2 adsorption-desorption isotherms performed on an AUTOSORB IQ Autosorb BET analyzer at 77 K. The chemical environment of each element was investigated by X-ray photoelectron spectroscopy (XPS, UL V AC PHI Quantera). The actual Fe content of Fe-SA/N-C was measured via inductively coupled plasma mass spectrometry (ICP-MS, PerkinElmer NexION 300X ICP). Atomic-level understandings of the coordination structure of the materials were conducted by X-ray absorption near-edge structure (XANES) and extended X-ray absorption fine structure (EXAFS) performed at 1W1B station in the Singapore Synchrotron Light Source (SSLS) center (operated at an energy of 2.5 GeV with an average electron current of < 200 mA).

1.2 Electrochemical characterization

Electrochemical measurements for ORR were conducted on a CHI 760E electrochemical potentiostat equipped with a PINE configuration, using a glassy carbon electrode (GCE) and carbon rod as the working and counter electrodes, respectively. The Hg/HgO electrode served as the reference electrode for the alkaline medium (0.1 M KOH aqueous solution). The Ag/AgCl electrode was served as the reference electrode for acid medium (0.5 M H_2SO_4 aqueous solution) and neutral medium (0.1 M PBS aqueous solution). To prepare the working electrode, freshly prepared catalyst ink (3 mg of catalyst homogeneously dispersed in the mixture of 10 μL of 5% Nafion solution, 375 μL of ethanol, and 125 μL of DI water) was carefully dropped onto the surface of GCE. After naturally evaporation, a uniform layer with a catalyst loading of 299 $\mu g \cdot cm^{-2}$ was obtained. Before the measurement, the Hg/HgO electrode was calibrated to the reversible hydrogen electrode (RHE) at 25 ^{o}C in 0.1 M KOH aqueous solutions. The ORR polarization curves were recorded at room temperature individually in the O_2-saturated 0.1 M KOH, 0.5 M H_2SO_4 and 0.1 M PBS aqueous solution at various rotation rates (400–2500 rpm). Methanol tolerance was tested by chronoamperometric measurements at 0.85, 0.75, and 0.55 V *vs*. RHE in an O_2-saturated mixed solution containing 0.1 M KOH, 0.5 M H_2SO_4, 0.1 M PBS aqueous solution, and an injection of 5 mL methanol. Polarization curves for OER were recorded in 0.1 M KOH aqueous solution at a scan rate of 5 $mV \cdot s^{-1}$. The potentials of the recorded polarization curves without *iR* compensation in this work were all converted to *vs*. RHE according to the equation: E(*vs*. RHE) = E (*vs*. Hg/HgO)

+ 0.89 V in 0.1 M KOH aqueous solution, E (*vs*. RHE) = E (*vs*. Ag/AgCl) +0.211 in 0.5 M H_2SO_4 aqueous solution and E (*vs*. RHE) = E (*vs*. Ag/AgCl) +0.635 in 0.1 M PBS aqueous solution.

The Koutecky-Levich (K-L) plots were analyzed at various electrode potentials. The electron transfer numbers of ORR were determined according to the K-L equation:

$$\frac{1}{j} = \frac{1}{j_L} + \frac{1}{j_K} = \frac{1}{B\omega^{1/2}} + \frac{1}{j_K} \quad (1)$$

$$B = 0.62nFC_0(D_0)^{2/3}v^{-1/6} \quad (2)$$

$$j_K = nFkC_0 \quad (3)$$

where j, j_K, and j_L are the measured, kinetic, and diffusion-limiting current densities, ω is the angular velocity of the disk ($\omega = 2\pi N$, N is the rotation speed), n is the electron transfer number, F is the Faraday constant (F = 96485 C·mol^{-1}), C_0 represents the bulk concentration of O_2 (C_0 = 1.2×10^{-6} mol·cm^{-3} in 0.1 M KOH aqueous solution), D_0 is the diffusion coefficient of O_2 (D_0 = 1.9×10^{-5} cm^2·s^{-1} in 0.1 M KOH aqueous solution), v is the kinematic viscosity of the electrolyte (v = 0.01 cm^2·s^{-1} in 0.1 M KOH aqueous solution), and k is the electron transfer rate constant. Similarly, commercial Pt/C was chosen with the same loading of 299 μg·cm^{-2} on the GCE for comparison. The electron transfer number (n) and peroxide yield (H_2O_2%) were calculated based on the disk current (I_{Disk}) and ring current (I_{Ring}) in RRDE measurement via the following equations:

$$n = 4I_{Disk}/(I_{Disk} + I_{Ring}/N) \quad (4)$$

$$Y_{H_2O_2/HO_2^-}(\%) = (200 \times I_{Ring}/N)/(I_{Disk} + I_{Ring}/N) \quad (5)$$

where $N = 0.37$ is the current collection efficiency of the Pt ring.

The electrochemically active surface area (ECSA) was calculated according to the following equation:

$$\text{ECSA} = C_{dl} / (C_s * \text{per cm}^2_{ECSA}) \quad (6)$$

where C_s (40 μF·cm^{-2}) refers to the atomically smooth planar surface capacitance, and the double-layer capacitance of C_{dl} is calculated from the CV curves in a non-faradic region of 1.15–1.25 V.

1.3 Fabrication of home-made Zn-air batteries

Liquid Zn-air batteries

A clean Zn plate with a thickness of 0.6 mm was employed as the anode of liquid ZAB. The KOH aqueous solution (6 M) dissolving 0.2 M $Zn(Ac)_2$ was used as the electrolyte. The cathode, an air electrode, comprises three layers following the order of nickel foam, polyphenylene sulfide (PPS) sheet, and carbon paper, which serve as current collector, gas diffusion layer, and catalyst carrier, respectively.

Flexible solid-state Zn-air batteries

Zn foil and PAA gel were served as the anode electrode and solid electrolyte, respectively, for the flexible solid-state ZABs. The composite carbon cloth served as an air electrode with a profile of 2 cm × 2 cm, comprising three layers in the order of nickel foam, PPS sheet, and carbon cloth. And the loading of catalyst on the composite carbon cloth is determined to be 0.58 mg·cm^{-1}. To prepare the PAA gel electrolyte: to 30 mL of DI water containing 22 g of KOH, 1 g of N,N-methylene

diacrylamide as a cross-linker containing 5 g of acrylic acid was quickly poured under continuous stirring, followed by dissolution 1.2 g of $Zn(Ac)_2$. After stirring for 1 h, 24 mL of DI water dissolved 0.12 g of $K_2S_2O_8$, serving as the initiator, was added to the aforementioned solution in the square mold and then shaken vigorously to form the PAA gel.

The specific capacity and energy density were calculated according to the following equations:

$$\text{Specific capacity (mAh·g}^{-1}) = I \times t/w_{Zn} \quad (7)$$

$$\text{Energy density (Wh·kg}^{-1}) = I \times V \times t/w_{Zn} \quad (8)$$

where I is the applied current (A), t is the serving time (s), V is the average discharge voltage (V), and w_{Zn} is the weight of zinc consumed (g).

2 Density functional theory (DFT) calculation

All theoretical calculations were implemented based on the Vienna Ab initio Simulation Package (VASP) using the projected-augmented wave (PAW) method.[1,2] The exchange-correlation energies were determined using the GGA method parameterized with the PBE functional. The Brillouin zone was sampled with Monkhorst-Pack mesh with a 2 × 2 × 1 *k*-point grid. Both geometry optimization and thermodynamic calculations were carried out with a convergence tolerance of 0.001 Å, force tolerance of 0.03 eV·Å^{-1}, and energy tolerance of 1.0×10^{-5} eV.

The free energies (G) of the reactants, intermediates, and products were obtained according to the following equation:

$$G = E_{total} + \text{ZPE} - \text{TS} \quad (9)$$

where E_{total} is the total energy of the species, ZPE is the zero point energy, and S is the entropy.

For ORR calculation in an alkaline environment, the four-electron pathway generally occurs according to the following steps:

(1) O_2 (g) + * + e^- + H_2O (l) → *OOH + OH^-

(2) *OOH + e^-→ *O + OH^-

(3) *O + H_2O (l) + e^- → *OH+ OH^-

(4) *OH + e^-→ OH^- + *

where * refers to an active site on the surface of the catalyst. *OH, *O, *OOH are the adsorbed intermediates.

The free energy change along the ORR processes can be derived as,

$$\Delta G_1 = \Delta G_{*OOH} - 4.92 \quad (10)$$

$$\Delta G_2 = \Delta G_{*O} - \Delta G_{*OOH} \quad (11)$$

$$\Delta G_3 = \Delta G_{*OH} - \Delta G_{*O} \quad (12)$$

$$\Delta G_4 = -\Delta G_{*OH} \quad (13)$$

3 Supplementary Figures and Tables

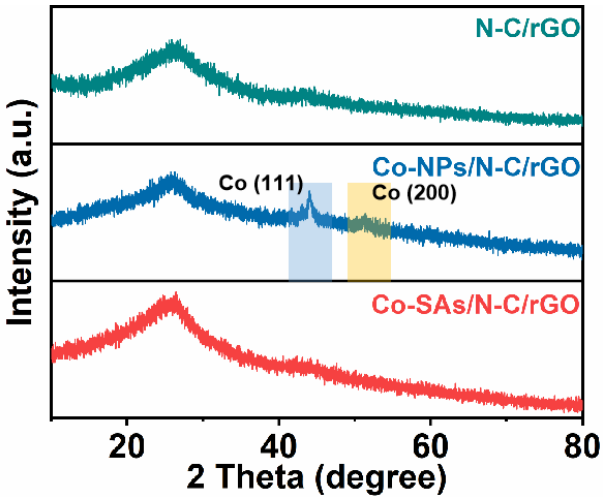

Figure S1 XRD patterns of N-C/rGO, Co-NPs/N-C/rGO, and Co-SAs/N-C/rGO.

Figure S2 Raman spectra of N-C/rGO, Co-NPs/N-C/rGO, and Co-SAs/N-C/rGO.

Figure S3 N_2 adsorption-desorption isotherm and the corresponding pore-size distribution curves (inset) of Co-SAs/N-C/rGO.

Figure S4 XPS survey spectra of Co-NPs/N-C/rGO and Co-SAs/N-C/rGO.

Figure S5 LSV curves of ORR for the Fe catalysts pyrolyzed from the different Zn/Co molar ratios (Zn/Co=10:1, 20:1, 40:1, 80:1, 160:1, respectively) at a rotating rate of 1600 rpm in O_2-saturated 0.1 M KOH aqueous solution.

Figure S6 Electrochemical impedance spectroscopy plots of Co-SAs/N-C/rGO and Co-N-C at 0.85 V *vs*. RHE in O_2 saturated 0.1 M KOH solution.

Figure S7 Polarization curves of Co-NPs/N-C/rGO and commercial Pt/C at varying rotating speeds in 0.1 M KOH aqueous solution; and corresponding K-L plots of at different potentials in the inset.

Figure S8 Stability test of Co-SAs/N-C/rGO, Co-NPs/N-C/rGO, and commercial Pt/C in 0.1 M KOH aqueous solution.

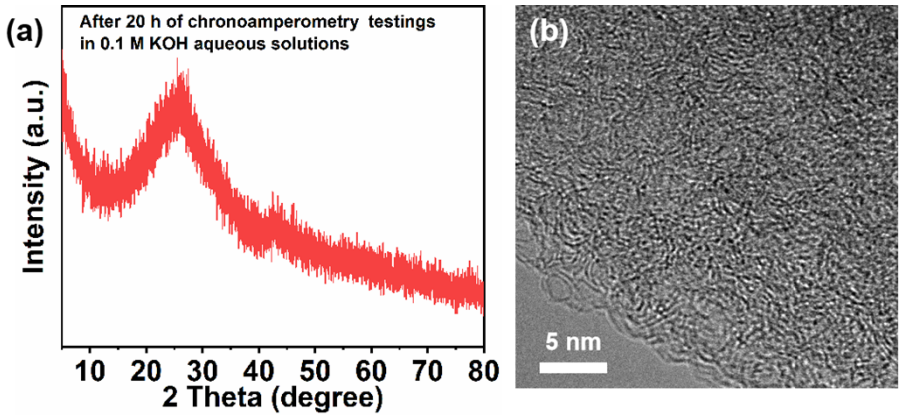

Figure S9 (a) XRD patterns, (b) HR-TEM images of Co-SAs/N-C/rGO after 20 h of chronoamperometry test in 0.1 M KOH aqueous solution.

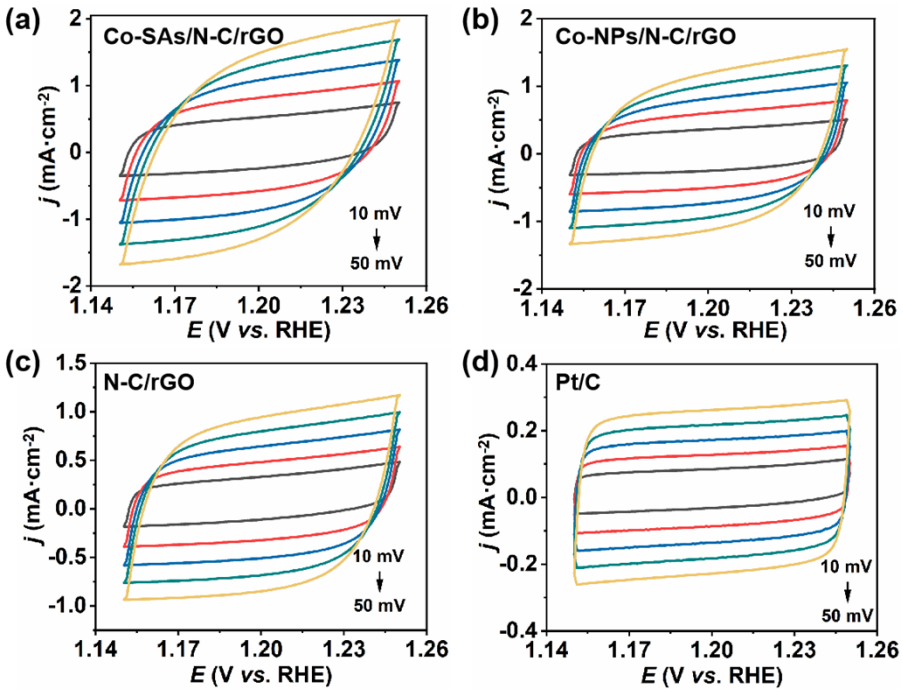

Figure S10 CV curves at various scan rates of (a) Co-SAs/N-C/rGO; (b) Co-NPs/N-C/rGO; (c) N-C/rGO; (d) commercial Pt/C in 0.1 M KOH aqueous solution.

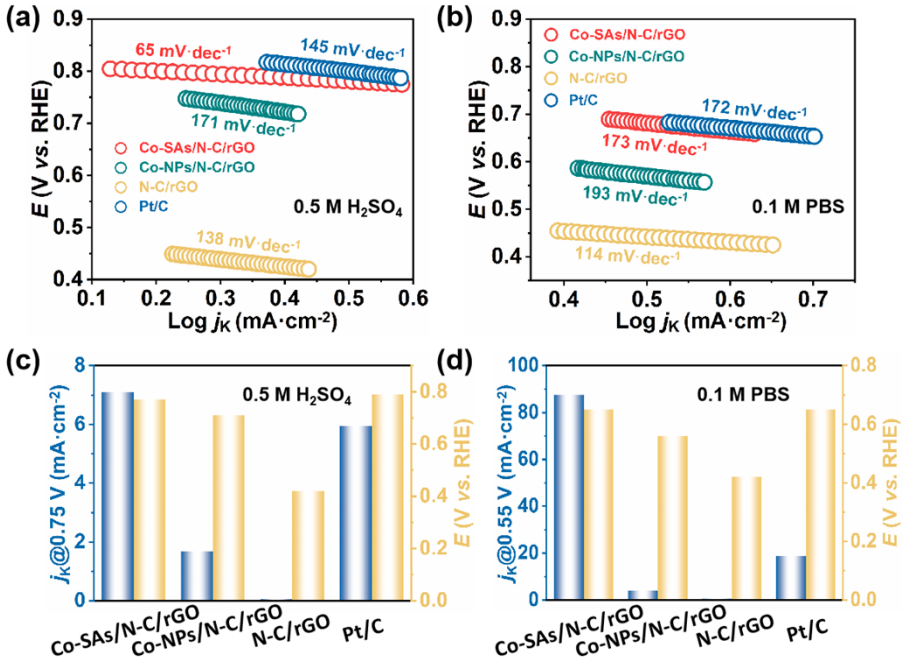

Figure S11 Tafel plots of N-C/rGO, Co-SAs/N-C/rGO, Co-NPs/N-C/rGO, and commercial Pt/C in O_2-saturated (a) 0.5 M H_2SO_4 aqueous solution and (b) 0.1 M PBS aqueous solution; j_K and $E_{1/2}$ of N-C/rGO, Co-SAs/N-C/rGO, Co-NPs/N-C/rGO, and commercial Pt/C in O_2-saturated (c) 0.5 M H_2SO_4 aqueous solution and (d) 0.1 M PBS aqueous solution.

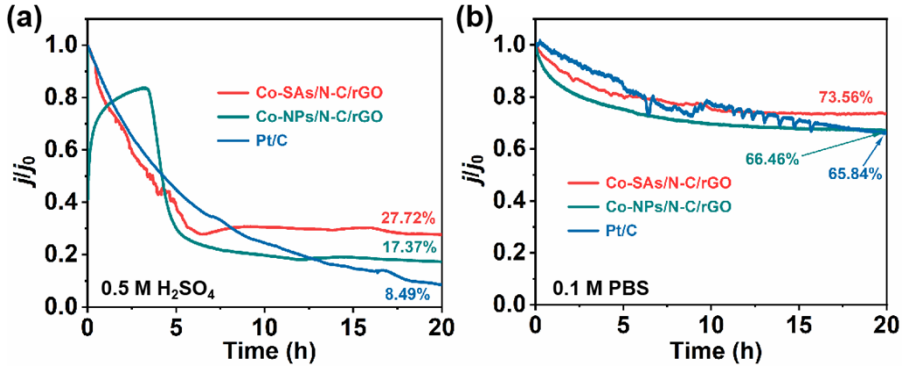

Figure S12 Stability test of Co-SAs/N-C/rGO, Co-NPs/N-C/rGO, and commercial Pt/C in (a) 0.5 M H_2SO_4 aqueous solution and (b) 0.1 M PBS aqueous solution.

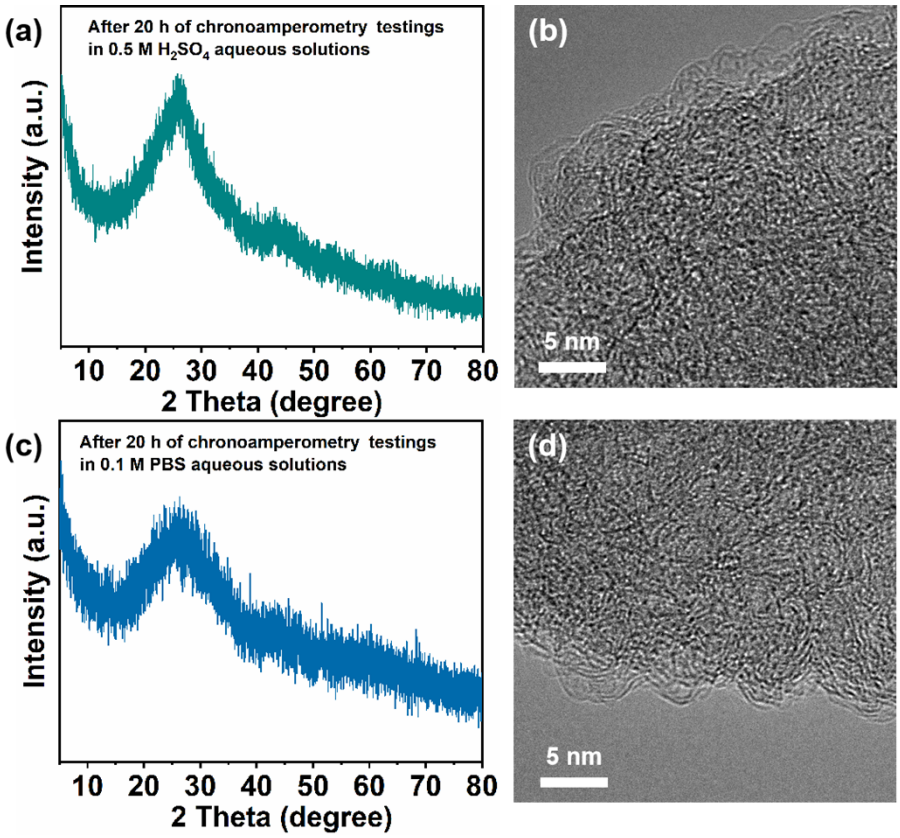

Figure S13 (a) XRD patterns, (b) HR-TEM images of Co-SAs/N-C/rGO after 20 h of chronoamperometry test in 0.5 M H_2SO_4 aqueous solution; (c) XRD patterns, (d) HR-TEM images of Co-SAs/N-C/rGO after 20 h of chronoamperometry test in 0.1 M PBS aqueous solution.

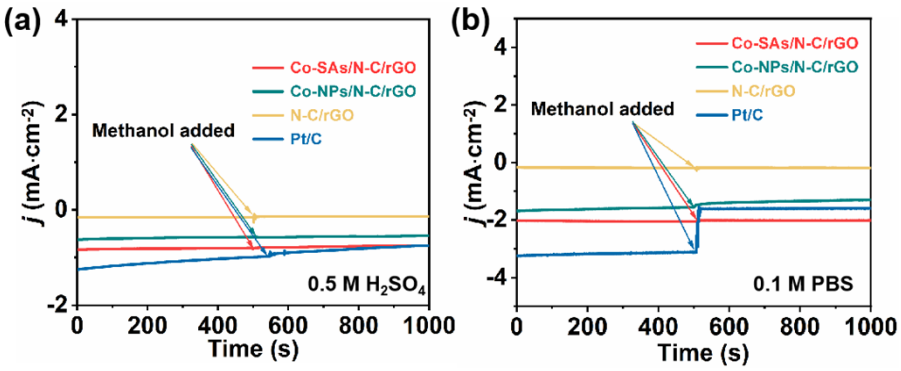

Figure S14 Methanol-tolerant test of N-C/rGO, Co-SAs/N-C/rGO, Co-NPs/N-C/rGO, and commercial Pt/C in (a) 0.5 M H_2SO_4 aqueous solution and (b) 0.1 M PBS aqueous solution.

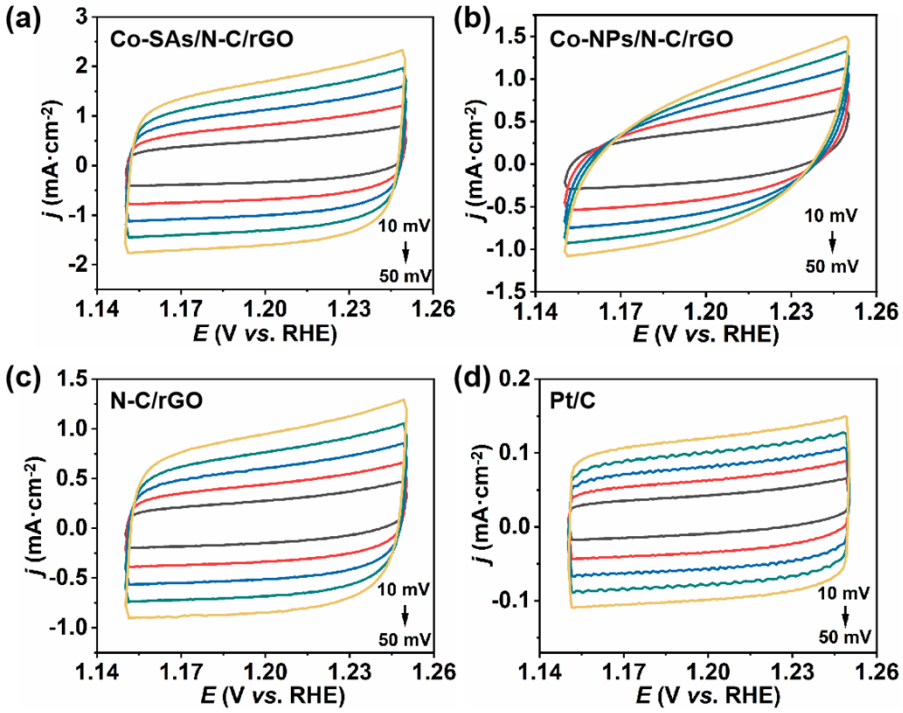

Figure S15 CV curves at various scan rates of (a) Co-SAs/N-C/rGO; (b) Co-NPs/N-C/rGO; (c) N-C/rGO; (d) commercial Pt/C in 0.5 M H_2SO_4 aqueous solution.

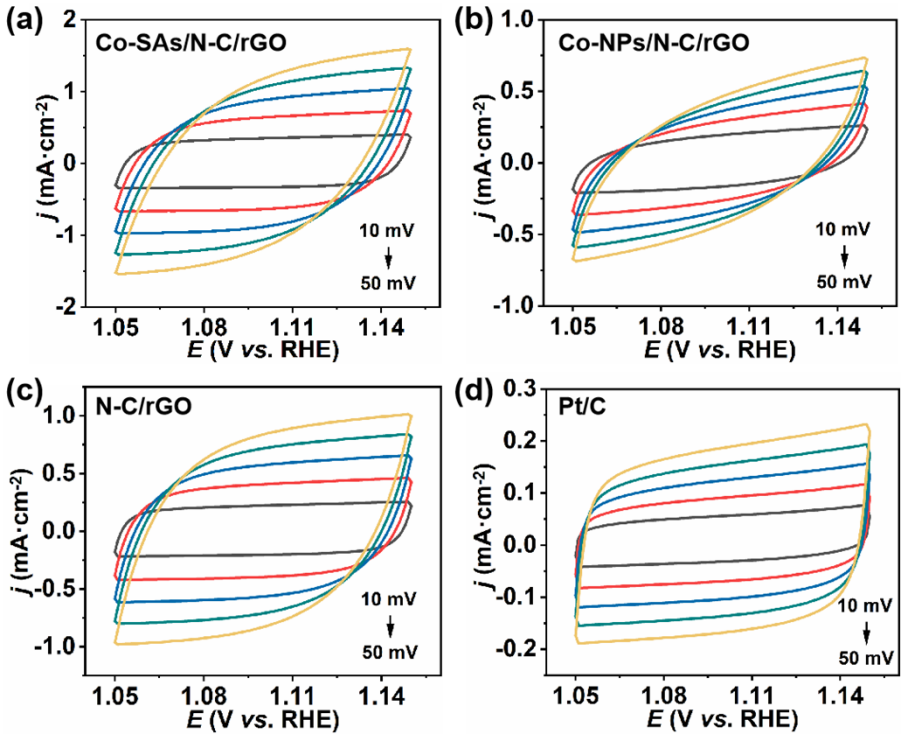

Figure S16 CV curves at various scan rates of (a) Co-SAs/N-C/rGO; (b) Co-NPs/N-C/rGO; (c) N-C/rGO; (d) commercial Pt/C in 0.1 M PBS aqueous solution.

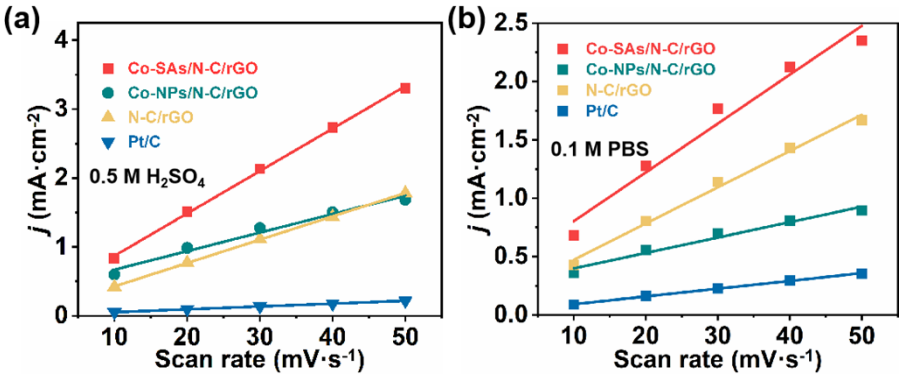

Figure S17 The extraction of the C_{dl} of N-C/rGO, Co-SAs/N-C/rGO, Co-NPs/N-C/rGO, and commercial Pt/C in (a) 0.5 M H_2SO_4 aqueous solution and (b) 0.1 M PBS aqueous solution.

Figure S18 Structural models of (a) CoN_4 and (b) CoNPs.

Table S1 EXAFS fitting parameters at the Co *K*-edge for various samples（S_0^2=0.718）

Sample	Shell	*CN*[a]	*R*(Å)[b]	σ^2(Å^2)[c]	ΔE_0(eV)[d]	*R* factor
			Co K-edge			
Co foil	Co-Co	12*	2.49±0.01	0.0062±0.0003	6.9	0.0028
CoPc	Co-N	4.3±0.5	1.92±0.04	0.0023±0.0007	11.6	0.0035
Co_3O_4	Co-O	5.9±0.5	1.91±0.03	0.0024±0.0015	0.1	0.0022
Co-SAs/N-C/rGO	Co-N	3.8±0.4	1.86±0.03	0.0085±0.0047	-5.9	0.0034

Table S2 Elemental analysis of Co-NPs/N-C/rGO and Co-SAs/N-C/rGO from XPS measurements.

Sample	C (at%)	N (at%)	O (at%)	Co (at%)	Zn (at%)
Co-NPs/N-C/rGO	76.82	12.71	5.24	1.35	3.88
Co-SAs/N-C/rGO	80.19	6.75	10.12	0.65	2.29

Table S3 Comparison of the ORR performance of the as-synthesized catalysts in O_2-saturated 0.1 M KOH, 0.5 M H_2SO_4 and 0.1M PBS solutions at 1600 rpm.

Catalysts	E_{onset} (V *vs.* RHE)	$E_{1/2}$ (V *vs.* RHE)	j_K (mA·cm^{-2})	j_L (mA·cm^{-2})	Electrolyte
			j_K@0.85		
Co-SAs/N-C/rGO	1.01	0.84	4.51	5.55	
Co-NPs/N-C/rGO	0.93	0.83	2.71	4.28	0.1 M KOH
N-C/rGO	0.86	0.75	0.16	3.75	
Pt/C	0.96	0.85	6.35	5.76	
			j_K@0.75		
Co-SAs/N-C/rGO	0.89	0.77	7.09	3.83	
Co-NPs/N-C/rGO	0.87	0.71	1.68	2.61	0.5 M H_2SO_4
N-C/rGO	0.68	0.42	0.05	2.73	
Pt/C	0.96	0.79	5.95	3.69	
			j_K@0.55		
Co-SAs/N-C/rGO	0.89	0.65	87.54	4.30	
Co-NPs/N-C/rGO	0.81	0.56	4.02	3.70	0.1 M PBS
N-C/rGO	0.67	0.42	0.54	4.40	
Pt/C	0.96	0.65	18.66	4.93	

Table S4 Comparison of ORR performance in alkaline media of Co-SAs/N-C/rGO at 1600 rpm with previously reported representative non-precious electrocatalysts.

Catalysts	E_{onset} (V *vs.* RHE)	$E_{1/2}$ (V *vs.* RHE)	ΔE (mV) ($E_{1/2}$-catalyst - $E_{1/2}$-Pt/C)	Elecrolyte	Ref.
Co-SAs/N-C/rGO	**1.01**	**0.84**	**-10**		**This work**
p-Fe-N-CNFs	0.91	0.82	0		3
Co@N-C700	/	0.78	-40		4
Co-CMS	0.88	0.83	0		5
S-Co/N/C	0.99	0.86	0		6
FeNi SAs/NC	0.98	0.84	/	0.1 M KOH	7
Co-FeCo/N-G	0.89	0.82	/		8
Fe–NiNC	1.00	0.84	/		9
Co/N–C-800	0.88	0.82	-50		10
Co-NC-AD	0.95	0.86	/		11
Co/CNT/MCP-850	0.94	0.80	-36		12

Table S5 Comparison of ORR performance in acidic media of Co-SAs/N-C/rGO at 1600 rpm with previously reported representative non-precious electrocatalysts.

Catalysts	E_{onset} (V *vs.* RHE)	$E_{1/2}$ (V *vs.* RHE)	ΔE (mV) ($E_{1/2}$-catalyst - $E_{1/2}$-Pt/C)	Elecrolyte	Ref.
Co-SAs/N-C/rGO	**0.89**	**0.77**	**-20**		**This work**
20Co-NC-1100	0.93	0.80	-50		13
CoNC-800	0.77	0.63	-60		14
UF Co-N-C	0.87	0.75	-50		15
Co-pyridinic N-C	0.93	0.83	-10	0.5 M H_2SO_4	16
Co–N/C+N_P+N_G	0.96	0.815	-15		17
S-POP	0.82	0.72	-90		18
NSPC-0.2–900	0.81	0.71	-80		19
ZnCo-NC-II	0.941	0.786	-64		20

Table S6 Comparison of ORR performance in neutral media of Co-SAs/N-C/rGO at 1600 rpm with reported representative non-precious electrocatalysts.

Catalysts	E_{onset} (V *vs.* RHE)	$E_{1/2}$ (V *vs.* RHE)	ΔE (mV) ($E_{1/2}$-catalyst - $E_{1/2}$-Pt/C)	Elecrolyte	Ref.
Co-SAs/N-C/rGO	**0.84**	**0.65**	**0**		**This work**
FeNPC	0.90	0.751	-61		21
Co-N-C-10	0.90	0.65	-50		22
FeNSC-ZM	1.00	0.66	150		23
Fe/NC-3	/	0.687	-49		24
Fe-N-C/800-HT2	0.862	0.743	-47		25
Fe_3O_4@N/Co-C	0.72	0.53	-60	0.1 M PBS	26
Fe-N-C-NH_3	0.86	0.65	-120		27
Co-C-16	0.715	0.630	-42		28
Fe,N/PGC-30	0.85	0.61	0		29
Fe@BC-800	0.86	0.68	-30		30
Cu-CTF/CP	0.81	0.59	-190		31

Table S7 Summary of performance based on PGM-free catalysts (the former) and commercial Pt/C (the latter) for liquid Zn-air batteries in an alkaline electrolyte.

Catalysts	OCV (V)	Power density ($mW \cdot cm^{-2}$)	Specific capacity ($mAh \cdot g^{-1}$)	Ref.
Co-SAs/N-C/rGO	**1.52/1.49**	**104.91/54.71**	**671.94/657.32**	**This work**
NiFe@C@Co CNFs	1.44/---	130/75	694/545	32
CoFe-SNC	1.45/1.45	76.5/66.9	636.3/587.06	33
Ir@Co_3O_4	---	163/194	712/675	34
CoFe-Co@PNC-12	1.45/1.43	152.8/73	786/762	35
Fe-N-C/N-OMC	1.55/1.44	113/81	711/582	36
Fe,Co-SA/CS	1.43/---	86.65/110.3	819.6/779.7	37
SA-Fe-3DOMC	1.48/1.37	140/124.5	786.6/---	38

Table S8 Summary of performance based on PGM-free catalysts for flexible solid-state Zn-air batteries in an alkaline electrolyte.

Catalysts	OCV (V)	Power density ($mW \cdot cm^{-2}$)	Ref.
Co-SAs/N-C/rGO	**1.36**	**74.61**	**This work**
CNT@POF	1.39	22.3	39
FeP/Fe_2O_3@NPCA	1.42	40.8	40
V_2O_3/MnS/CC	1.40	72	41
NBSCF nanofibers	1.44	18.59	42
FeCo/Se-CNT	1.405	3.75	43
1 nm-CoO_x/N-RGO	1.39	--	44

Table S9 The Gibbs free energies (eV) of each elementary reaction step at different potentials.

	*	*OOH	*O	*OH	*
Co-SA@0 V	4.92	3.99	2.58	0.78	0
Co-SA@1.23 V	0	0.30	0.12	-0.45	0
Co-NP@0 V	4.92	4.38	2.69	1.09	0
Co-NP@1.23 V	0	0.69	0.23	-0.14	0

References

1 G. Kresse and J. Furthmüller, *Comp. Mater. Sci*., 1996, **6**, 15–50.

2 P. E. Blöchl, *Phys. Rev. B*, 1994, **50**, 17953–17979.

3 B. C. Hu, Z. Y. Wu, S. Q. Chu, H. W. Zhu, H. W. Liang, J. Zhang and S. H. Yu, *Energy Environ. Sci*., 2018, **11**, 2208−2215.

4 H. B. Li, M. D. Zhang, W. Zhou, J. G. Duan and W. Q. Jin, *Chem. Eng. J*., 2021, **421**, 129719.

5 S. Liang, L. C. Zou, L. J. Zheng, F. Li, X. X. Wang, L. N. Song and J. J. Xu, *Adv. Energy Mater*., 2022, **12**, 2103097.

6 T. Sun, W. Zang, H. Yan, J. Li, Z. Zhang, Y. Bu, W. Chen, J. Wang, J. Lu and C. Su, *ACS Catal.*, 2021, **11**, 4498–4509.

7 D. S. Yu, Y. C. Ma, F. Hu, C. C. Lin, L. L. Li, H. Y. Chen, X. P. Han and S. J. Peng, *Adv. Energy Mater*., 2021, **11**, 2101242.

8 Q. Y. Jin, B. Ren, J. P. Chen, H. Cui and C. X. Wang, *Appl. Catal. B,* 2019, **256**, 117887.

9 X. F. Zhu, D. T. Zhang, C. J. Chen, Q. R. Zhang, R. S. Liu, Z. H. Xia, L. M. Dai, R. Amal and X. Y. Lu, *Nano Energy*, 2020, **71**, 104597.

10 X. Z. Fan, X. Du, Q. Q. Pang, S. Zhang, Z. Y. Liu and X. Z. Yue, *ACS Appl. Mater. Interfaces,* 2022, **14**, 8549–8556.

11 Y. Feng, K. X. Song, W. Zhang, X. Y. Zhou, S. J. Yoo, J. G. Kim, S. F. Qiao, Y. G. Qi, X. Zou, Z. J. Chen, T. T. Qin, N. L. Yue, Z. Z. Wang, D. B. Li and W. T. Zheng, *J. Energy Chem*., 2022, **70**, 211–218.

12 X. W. Zhou, X. Liu, J. H. Zhang, C. Zhang, S. J. Yoo, J. G. Kim, X. Y. Chu, C. Song, P. Wang, Z. Z. Zhao, D. B. Li, W. Zhang and W. T. Zheng, *Carbon*, 2020, **166**, 284–290.

13 X. X. Wang, D. A. Cullen, Y. T. Pan, S. Hwang, M. Y. Wang, Z. X. Feng, J. Y. Wang, M. H. Engelhard, H. G. Zhang, Y. H. He, Y. Y. Shao, D. Su, K. L. More, J. S. Spendelow and G. Wu, *Adv. Mater.*, 2018, **30**, 1706758.

14 H. Jiang, Y. S. Liu, J. Y. Hao, Y. Q. Wang, W. Z. Li and J. Li, *ACS Sustainable Chem. Eng*., 2017, **5**, 5341–5350.

15 H. Ye, L. J. Li, D. D. Liu, Q. J. Fu, F. Z. Zhang, P. C. Dai, X. Gu and X. B. Zhao, *ACS Appl. Mater. Interfaces,* 2020, **12**, 57847–57858.

16 Y. Ha, B. Fei, X. X. Yan, H. B. Xu, Z. L. Chen, L. X. Shi, M. S. Fu, W. Xu and R. B. Wu, *Adv. Energy Mater.*, 2020, **10**, 2002592.

17 X. R. Zhang, X. M. Xu, S. X. Yao, C. Hao, C. Pan, X. Xiang, Z. Q. Tian, P. K. Shen, Z. P. Shao and S. P. Jiang, *Small*, 2022, **18**, 2105329.

18 W. Yan, S. F. Cao, Z. X. Xiao, F. Dai, T. Xing, Z. Li, Y. L. Chen, X. Q. Lu and X. Y. Li, *Electrochim Acta*, 2021, **377**, 138107.

19 L. Q. Wang, K. X. Liang, L. Deng and Y. N. Liu, *Appl. Catal. B,* 2019, **246**, 89–99.

20 K. X. Song, Y. Feng, X. Y. Zhou, T. T. Qin, X. Zou, Y. G. Qi, Z. J. Chen, J. C. Rao, Z. Z. Wang, N. L. Yue, X. Ge, W. Zhang and W. T. Zheng, *Appl. Catal. B*, 2022, **316**, 121591.

21 L. L. Fan, X. F. Wei, X. T. Li, Z. N. Liu, M. F. Li, S. Liu, Z. X. Kang, F. N. Dai, X. Q. Lu and D. F. Sun, *Nano Res.*, 2022, https://doi.org/10.1007/s12274-022-4939-5.

22 X. G. Feng, X. X. Xiao, J. D. Zhang, L. P. Guo and Y. Xiong, *Electrochim. Acta*, 2021, **389**, 138791.

23 Y. Q. Dong, Z. Fang, D. Ou, Q. Shi, Y. Ma, W. Y. Yang, B. Tang and Q. Liu, *Chem. Eng. J.*, 2022, **444**, 136433.

24 M. J. Liu, J. Lee, T. C. Yang, F. Y. Zheng, J. Zhao, C. M. Yang and L. Y. S. Lee, *Small Methods,* 2021, **5**, 2001165.

25 G. Zhang, L. Li, M. Chen and F. Yang, *J. Mater. Chem. A,* 2020, **8**, 9256–9267.

26 C. Cao, L. Wei, M. Su, G. Wang and J. Shen, *J. Mater. Chem. A*, 2016, **4**, 9303–9043.

27 Z. Chen, D. Zhao, C. Chen, Y. Xu, C. Sun, K. Zhao, M. A. Khan, D. Ye, H. Zhao, J. Fang, X. A. Sun and J. Zhang, *J. Colloid Interface Sci*., 2021, 582, 1033–1040.

28 Y. Xu, H. Zhang, P. Zhang, M. Lu, X. Xie and L. Huang, *J. Mater. Chem. A*, 2021, **9**, 10695–10703.

29 W. Gu, L. Hu, J. Li and E. Wang, *J. Mater. Chem. A*, 2016, **4**, 14364–14370.

30 X. Ma, Z. Lei, W. Feng, Y. Ye, and C. Feng, *Carbon*, 2017, **123**, 481–491.

31 K. Iwase, T. Yoshioka, S. Nakanishi, K. Hashimoto and K. Kamiya, *Angew. Chem. Int. Ed.*, 2015, **54**, 11068–11072.

32 X. Chen, J. Pu, X. H. Hu, Y. C. Yao, Y. B. Dou, J. Y. Jiang and W. J. Zhang, *Small*, 2022, **18**, 2200578.

33 C. C. Weng, J. T. Ren, H. Y. Wang, X. W. Lv, Y. J. Song, Y. S. Wang, L. Chen, W. W. Tian and Z. Y. Yuan, *Appl. Catal. B*, 2022, **307**, 121190.

34 Y. W. Dai, J. Yu, J. Wang, Z. P. Shao, D. Q. Guan, Y. C. Huang and M. Ni, *Adv. Funct. Mater.*, 2022, **32**, 2111989.

35 Z. Lei, Y. Y. Tan, Z. Y. Zhang, W. Wu, N. C. Cheng, R. Z. Chen, S. C. Mu and X. L. Sun, *Nano Res*., 2021, **14**, 868−878.

36 J. X. Han, H. L. Bao, J. Q. Wang, L. R. Zheng, S. R. Sun, Z. L. Wang and C. W. Sun, *Appl. Catal. B*, 2021, **280**, 119411.

37 V. Jose, H. M. Hu, E. Edison, W. M. Jr, H. Ren, P. Kidkhunthod, S. Sreejith, A. Jayakumar, J. M. V. Nsanzimana, M. Srinivasan, J. Choi and J. M. Lee, *Small Methods*, 2021, **5**, 2000751.

38 P. B. Li, X. Q. Qi, L. Zhao, J. J. Wang, M. Wang, M. H. Shao, J. S. Chen, R. Wu and Z. D. Wei, *J. Mater. Chem. A*, 2022, **10**, 5925−5929.

39 B. Q. Li, S. Y. Zhang, B. Wang, Z. J. Xia, C. Tang and Q. Zhang, *Energy Environ. Sci*., 2018, **11**, 1723–1729.

40 K. Z. Wu, L. Zhang, Y. F. Yuan, L. X. Zhong, Z. X. Chen, X. Chi, H. Lu, Z. H. Chen, R. Zou, T. Z. Li, C. Y. Jiang, Y. K. Chen and X. W. Peng and J. Lu, *Adv. Mater*., 2020, **32**, 2002292.

41 Y. Rao, W. L. Li, S. Chen, Q. Yue, Y. N. Zhang and Y. J. Kang, *Small*, 2022, **18**, 2104411.

42 D. Lee, H. Lee, O. Gwon, O. Kwon, H. Y. Jeong, G. Kim and S. Y. Lee, *J. Mater. Chem. A,* 2019, **7**, 24231–24238.

43 H. W. Zhang, M. Q. Zhao, H. R. Liu, S. R. Shi, Z. H. Wang, B. Zhang, L. Song, J. Z. Shang, Y. Yang, C. Ma, L. R. Zheng, Y. Han and W. Huang, *Nano Lett*., 2021, **21**, 2255–2264.

44 T. P. Zhou, W. F. Xu, N. Zhang, Z. Du, C. A. Zhong, W. S. Yan, H. X. Ju, W. S. Chu, H. Jiang, C. Z. Wu and Y. Xie, *Adv. Mater*., 2019, **31**, 1807468.